Magnetic Reconnection in the Near Venusian Magnetotail
T. L. Zhang *et al.*
Science **336**, 567 (2012);
DOI: 10.1126/science.1217013

(see Fig. 1H); the data for the upper branch cannot be obtained because of interference from other signals (possibly the electron-like band). The QPI signature of the third band h_1 becomes unidentifiable within -6 ± 1.5 meV below E_F in the superconducting phase, consistent with the opening of a gap of this magnitude (Figs. 2E and 3E), but we cannot yet resolve any gap modulations.

The magnitude, anisotropy, and relative position of $\Delta_i(\vec{k})$ on bands h_3, h_2, and h_1 are then determined from Fig. 3, D and E, using the previously described procedure [(2), section III]. The resulting anisotropic superconducting gaps on bands h_3, h_2, and h_1 of LiFeAs are displayed in Fig. 4, A and B. Although our $g(|\vec{q}|,E)$ agree well with pioneering QPI studies of LiFeAs where common data exist, no studies of $\Delta_i(\vec{k})$ were reported therein (30). Moreover, although field-dependent Bogoliubov QPI can reveal OP symmetry (11), these techniques were not applied here to LiFeAs, and no OP symmetry conclusions were drawn herein. The anisotropic Δ_i reported recently in ARPES studies of LiFeAs (16, 17) appear in agreement with our observations for the h_3 (Fig. 1, γ) and h_2 (Fig. 1, α_2) bands. Lastly, our measurements are quite consistent with deductions on LiFeAs band structure from quantum oscillation studies (31). Overall, the growing confidence and concord in the structure of $\Delta_i(\vec{k})$ for LiFeAs will advance the quantitative theoretical study of the mechanism of its Cooper pairing. Moreover, the multiband anisotropic-gap QPI techniques introduced here will allow equivalent $\Delta_i(\vec{k})$ observations in other iron-pnictide superconductors.

References and Notes

1. P. J. Hirschfeld, M. M. Korshunov, I. I. Mazin, *Rep. Prog. Phys.* **74**, 124508 (2011).
2. Materials and methods are available as supplementary materials on *Science* Online.
3. F. Wang, H. Zhai, Y. Ran, A. Vishwanath, D.-H. Lee, *Phys. Rev. Lett.* **102**, 047005 (2009).
4. T. A. Maier, S. Graser, D. J. Scalapino, P. J. Hirschfeld, *Phys. Rev. B* **79**, 224510 (2009).
5. R. Thomale, C. Platt, J. Hu, C. Honerkamp, B. A. Bernevig, *Phys. Rev. B* **80**, 180505R (2009).
6. S. Raghu, X.-L. Qi, C.-X. Liu, D. J. Scalapino, S.-C. Zhang, *Phys. Rev. B* **77**, 220503R (2008).
7. R. Sknepnek, G. Samolyuk, Y.-B. Lee, J. Schmalian, *Phys. Rev. B* **79**, 054511 (2009).
8. S. Maiti, A. V. Chubukov, *Phys. Rev. B* **82**, 214515 (2010).
9. H. Kontani, S. Onari, *Phys. Rev. Lett.* **104**, 157001 (2010).
10. A. D. Christianson et al., *Nature* **456**, 930 (2008).
11. T. Hanaguri, S. Niitaka, K. Kuroki, H. Takagi, *Science* **328**, 474 (2010).
12. B. Zeng et al., *Nat. Comms.* **1**, 112 (2010).
13. J.-Ph. Reid et al., *Phys. Rev. B* **82**, 064501 (2010).
14. M. A. Tanatar et al., *Phys. Rev. Lett.* **104**, 067002 (2010).
15. S. V. Borisenko et al., *Phys. Rev. Lett.* **105**, 067002 (2010).
16. S. V. Borisenko et al., *Symmetry* **4**, 251 (2012).
17. K. Umezawa et al., *Phys. Rev. Lett.* **108**, 037002 (2012).
18. Q.-H. Wang, D.-H. Lee, *Phys. Rev. B* **67**, 020511R (2003).
19. L. Capriotti, D. J. Scalapino, R. D. Sedgewick, *Phys. Rev. B* **68**, 014508 (2003).
20. T. S. Nunner, W. Chen, B. M. Andersen, A. Melikyan, P. J. Hirschfeld, *Phys. Rev. B* **73**, 104511 (2006).
21. Y.-Y. Zhang et al., *Phys. Rev. B* **80**, 094528 (2009).
22. A. Akbari, J. Knolle, I. Eremin, R. Moessner, *Phys. Rev. B* **82**, 224506 (2010).
23. S. Sykora, P. Coleman, *Phys. Rev. B* **84**, 054501 (2011).
24. I. I. Mazin, S. A. J. Kimber, D. N. Argyriou, *Phys. Rev. B* **83**, 052501 (2011).
25. X. C. Wang et al., *Solid State Commun.* **148**, 538 (2008).
26. M. J. Pitcher et al., *J. Am. Chem. Soc.* **132**, 10467 (2010).
27. C. W. Chu et al., *Physica C* **469**, 326 (2009).
28. D. J. Singh, *Phys. Rev. B* **78**, 094511 (2008).
29. T. Hanaguri et al., *Meeting Abstracts of the Phys. Soc. of Japan*, **65**, 617 (2010).
30. T. Hänke et al., *Phys. Rev. Lett.* **108**, 127001 (2012).
31. C. Putzke et al., *Phys. Rev. Lett.* **108**, 047002 (2012).

Magnetic Reconnection in the Near Venusian Magnetotail

T. L. Zhang,[1,2]* Q. M. Lu,[1] W. Baumjohann,[2] C. T. Russell,[3] A. Fedorov,[4] S. Barabash,[5] A. J. Coates,[6] A. M. Du,[7] J. B. Cao,[8] R. Nakamura,[2] W. L. Teh,[2] R. S. Wang,[2] X. K. Dou,[1] S. Wang,[1] K. H. Glassmeier,[9] H. U. Auster,[9] M. Balikhin[10]

Observations with the Venus Express magnetometer and low-energy particle detector revealed magnetic field and plasma behavior in the near-Venus wake that is symptomatic of magnetic reconnection, a process that occurs in Earth's magnetotail but is not expected in the magnetotail of a nonmagnetized planet such as Venus. On 15 May 2006, the plasma flow in this region was toward the planet, and the magnetic field component transverse to the flow was reversed. Magnetic reconnection is a plasma process that changes the topology of the magnetic field and results in energy exchange between the magnetic field and the plasma. Thus, the energetics of the Venus magnetotail resembles that of the terrestrial tail, where energy is stored and later released from the magnetic field to the plasma.

Magnetic reconnection is an important process in many astrophysical plasma environments, which leads to efficient and fast conversion of magnetic energy into kinetic energy of plasma particles. As a result of the rapid reconfiguration of the magnetic topology, it also transfers mass between different astrophysical plasma regimes. In particular, reconnection is associated with the formation of solar coronal mass ejections (1) and plasmoid ejections from the magnetotails of Earth, Jupiter, Saturn, and Mercury (2–5), all of which lead to substantial plasma loss. Magnetic reconnection may also be responsible for comet tail disconnection, which releases much of a comet's plasma tail into space (6, 7). Although understanding atmospheric loss is a key to establishing the evolutionary history of planets, the role of magnetic reconnection is still poorly understood because of the scarcity of in situ observations at planets other than Earth.

Three mechanisms of atmospheric loss have been identified at Venus: $V \times B$ pick-up processes (where V is velocity and B is the magnetic field), $J \times B$ acceleration in the plasma sheet (where J is current density), and the polar wind–type process in the tail boundary layer (8). Recent Venus Express data (9) reveal escape through the plasma sheet of the magnetotail and the tail boundary layer. Here, we show that reconnection is another acceleration mechanism, a situation not expected in the induced tail of Venus.

[1]Chinese Academy of Sciences Key Laboratory of Geospace Environment, University of Science and Technology of China, Hefei 230026, China. [2]Space Research Institute, Austrian Academy of Sciences, Graz 8042, Austria. [3]Institute of Geophysics and Planetary Physics, University of California, Los Angeles (UCLA), CA 90095–1567, USA. [4]Centre d'Etude Spatiale des Rayonnements, Toulouse 31028, France. [5]Swedish Institute of Space Physics, Kiruna 98128, Sweden. [6]Mullard Space Science Laboratory, University College London, London RH5 6NT, UK. [7]Institute of Geology and Geophysics, Chinese Academy of Sciences, Beijing 100029, China. [8]Space Science Institute, Beihang University, Beijing 100191, China. [9]Institut für Geophysik und Extraterrestrische Physik, Technische Universität Braunschweig, Braunschweig 38106, Germany. [10]Department of Automatic Control and Systems Engineering, University of Sheffield, Sheffield S1 3JD, UK.

*To whom correspondence should be addressed. E-mail: tielong.zhang@oeaw.ac.at

Fig. 1. A rotational magnetic field structure in the Venus magnetotail based on magnetic field measurements by Venus Express on 15 May 2006. The measurements (*22*) are in the planet-centered Venus Solar Orbital (VSO) coordinate system, with X sunward and Z toward orbital north, similar to the Geocentric Solar Ecliptic coordinate system at Earth. The shaded area represents Venus.
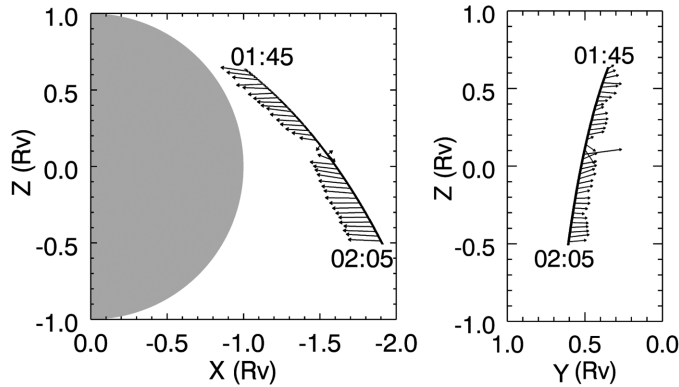
On 15 May 2006, a rotational magnetic field structure was observed by Venus Express when crossing the Venusian magnetotail (Fig. 1). The structure was located ~1.5 R_V (1 R_V = 6051 km, one Venus radius) down the tail and lasted ~3 min (0153 to 0156 UT). The event occurred during a time of enhanced interplanetary magnetic field (IMF) strength with small directional variation.

Because Venus has no intrinsic magnetic field, the configuration of its induced magnetosphere is controlled by the upstream IMF orientation and its draping around the highly conducting ionosphere. When we rotate the magnetic field observations from the measurement system to a system oriented with the expected electric field

Fig. 2. Plasmoid flux rope observed with magnetic field and plasma measurements on 15 May 2006. (**A** to **D**) The magnetic field data were rotated into a natural coordinate system with *x* along the ambient magnetic field before and after the events, *y* containing the bimodal perturbation, and *z* along the unimodal perturbation. The rotated coordinates are *x* = (0.863 −0.500 0.075), *y* = (0.213 0.224 −0.951), and *z* = (0.459 0.837 0.300). The dashed vertical lines are the edges of the plasmoid defined by the diamagnetic field minima at 0153:45 UT and 0155:19 UT. (**E** and **F**) The total counts of energetic electrons measured by the Electron Spectrometer (ELS) sensor and the total counts of the proton of the Ion Mass Analyzer (IMA) sensor (*23*), respectively. In these spectrograms, the IMA has 12 s time resolution, and the ELS has 4 s resolution. The termination of the ion counts at 0154:17 is due to a rotation of the spacecraft, which moved the look-direction of the ion sensor. The electron sensor is not as sensitive to spacecraft rotation as the ion sensor.
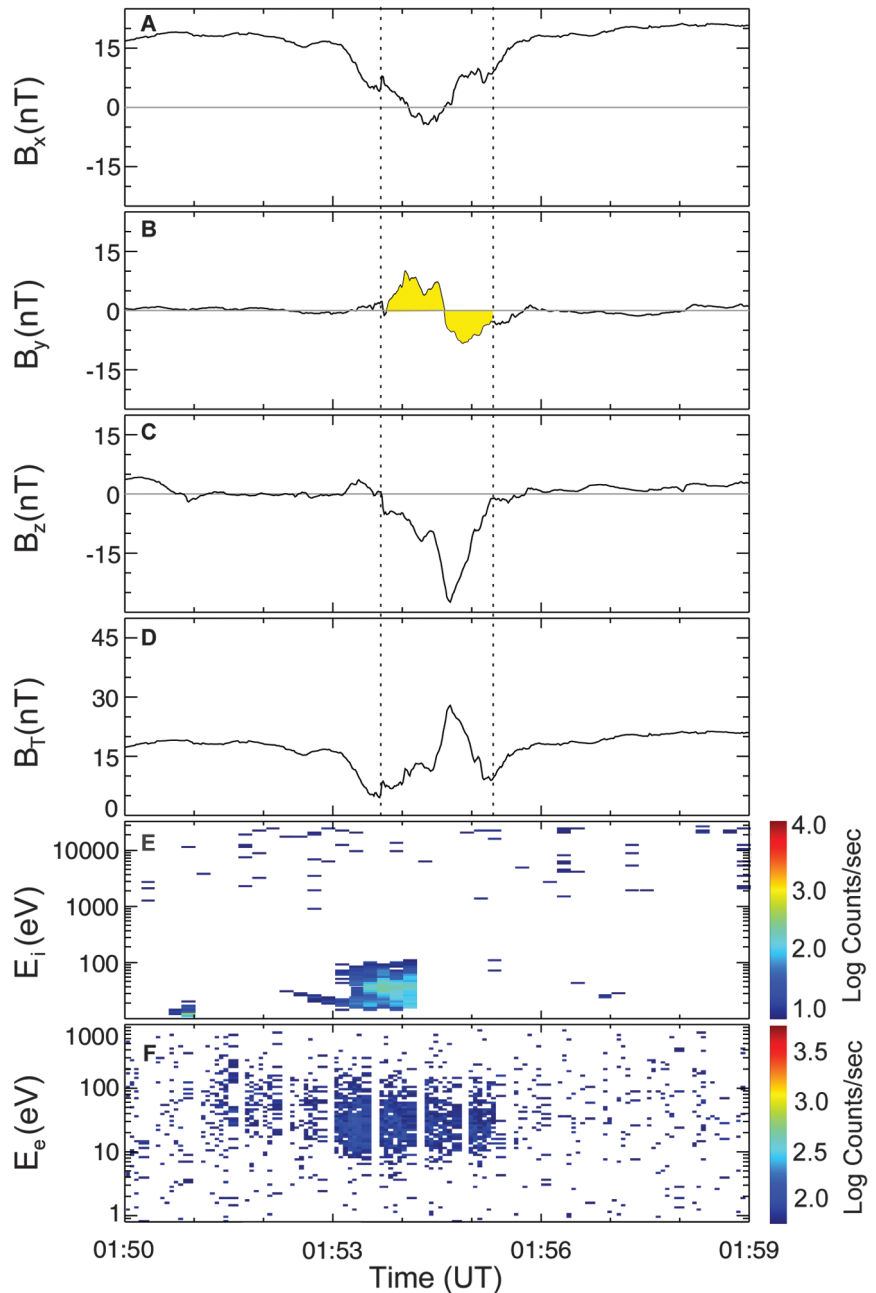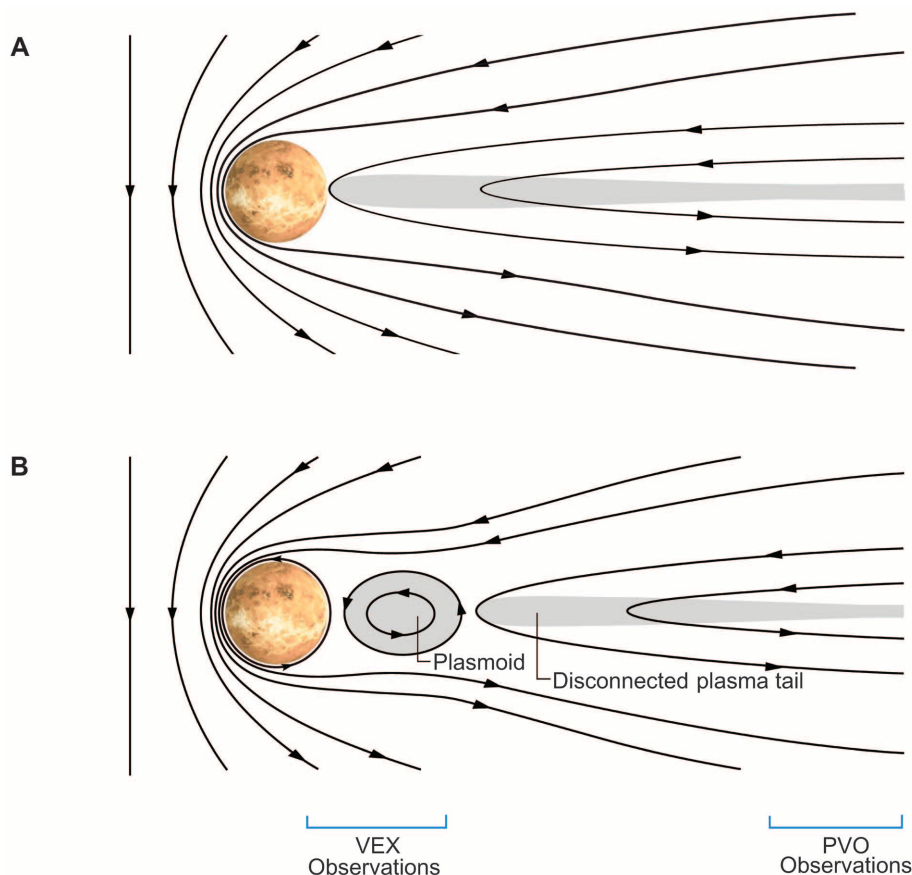
Fig. 3. Schematic illustration of the plasmoid formation and disconnected plasma tail events during the magnetic reconnection observed in the near Venusian tail. Field lines are indicated by solid lines. (**A**) Venusian magnetotail before magnetic reconnection and plasmoid formation. (**B**) The ionosphere was magnetized with a field line going all the way around the planet. The flux rope/O-line (plasmoid) was separated from the nightside magnetized ionosphere by a magnetic X-line. The more distant side of the O-line was separated from the disconnected plasma sheet by another X-line. The tail plasma sheet shedded O-lines toward the planet. The O-lines ran into the magnetized nightside, magnetically connected with it, and created first oval field lines and then circular field lines in the lower ionosphere. Later arriving O-lines reinforced the field. The region of observations by the Pioneer Venus mission (PVO) was in the distant tail, in contrast to Venus Express (VEX), which observed the near tail.

and the ambient magnetic directions (Fig. 2), the magnetic temporal variation is that of a well-defined flux rope plasmoid moving over the spacecraft. The structure has a bipolar-like rotation of the field and magnetic field maximum centered near the inflection point of the bipolar signature (*10*). The edges of the flux rope are well defined by diamagnetic field minima at 01:53:45 UT and 01:55:19 UT. A very strong plasmoid core field peaked at 27.8 nT, which is 46% higher than the neighboring lobe field of 19 nT. The enhanced ion and electron flux signatures were coincident with the plasmoid structure (Fig. 2, E and F). Simple integration as a moment of distribution function gives a bulk velocity of (31, –18, 7) km/s in VSO coordinates, revealing the Venus-ward motion of the plasmoid structure. The plasmoid duration was 94 s (from magnetic field measurements), implying its size was 3400 km, assuming the bulk velocity was the same as the plasmoid speed.

A plasmoid is a transient magnetic loop structure formed by magnetic reconnection in a planetary magnetotail. It is ubiquitous in planets with an intrinsic magnetic field such as Earth, Jupiter, Saturn, and Mercury (*2–5*), but it is not expected in the magnetotail of an unmagnetized planet such as Venus. We further looked through the Venus Express magnetic field data, identifying the negative B_Y in the current sheet in the magnetic field coordinate system. In this system, the current sheet is in the xz plane and IMF in the xy plane pointing to $+y$ direction, thus a negative B_Y in the current sheet can be regarded as the signature of reconnection, which is similar to the indication by a negative B_Z in the Earth's magnetotail plasma sheet. We found that the negative B_Y in the current sheet occurs quite frequently, predominantly in the $-E$ hemisphere, where the magnetic field draping pattern is more wrapped around the planet and the field reversal is dominant (*11*). Furthermore, the Venus-ward bulk flows

are found mostly within 2 R_V down the tail. Observations of Venus Express data imply that reconnection can operate in a quasi-steady-state in the near tail at Venus, at least during current conditions. Thus, the magnetic field is not just a buffer between the solar wind flow and the planetary atmosphere and ionosphere; rather, it provides a pathway for channelling a fraction of the incident energy flux of the solar wind into the night side atmosphere much like the situation in the terrestrial magnetotail.

The plasmoid in the Venus magnetotail as observed in this study is illustrated schematically in Fig. 3. When the magnetic record shown in Fig. 2 began, the spacecraft was between the planet and the magnetic island and the "rope" contained within it. As the event proceeded, the rope moved toward Venus and across the spacecraft (*12*). Venus' induced magnetosphere serves as an obstacle to the solar wind in the same way the Earth's magnetosphere does (*13*), but it occupies much smaller space volume, with a scaling factor of ~10. Magnetic reconnection occurs in the Earth's magnetotail and plasma sheet at ~10 to 30 Earth radii in the antisolar direction. By simple scaling, the equivalent region at Venus would be 1 to 3 R_V down the tail. That is exactly the region where Venus Express detected reconnection events. Because of its orbital geometry, the earlier Pioneer Venus mission (PVO) observed mainly the distant tail region at 8 to 12 R_V (*14*, *15*) and was thus unable to sample the right region.

The first observational estimate of the atmospheric loss of Venus was obtained by integrating the outflow plasma in the magnetotail on the basis of Venus Express observations (*16*). In this analysis, based on the reconstruction of the full distribution function, only regions in which the outward flux becomes stable were considered, and only the total outward flux regardless of the acceleration mechanism was taken into account. Any inward flux will not affect the total escape rate. However, if the plasma reaches the ionosphere and becomes deposited there, this interaction should lead to greater magnetization of the nightside ionosphere as well as heating and plasma transport. In this case, the plasma circulation may be like that recently considered for the Earth magnetosphere (*17*). Thus, despite their very different magnetic envelopes, the plasma dynamics of Venus and Earth display many similar characteristics.

References and Notes
1. P. F. Chen, *Liv. Rev. Sol. Phys.* **8**, 1 (2011).
2. C. T. Russell, in *Correlated Interplanetary and Magnetospheric Observations*, D. E. Page, Ed. (Reidel, Dordrecht, Netherlands, 1974), pp. 3–47.
3. C. T. Russell, K. K. Khurana, D. E. Huddleston, M. G. Kivelson, *Science* **280**, 1061 (1998).
4. C. M. Jackman *et al.*, *Geophys. Res. Lett.* **34**, L11203 (2007).
5. J. A. Slavin *et al.*, *Science* **324**, 606 (2009).
6. C. T. Russell, M. A. Saunders, J. L. Phillips, J. A. Fedder, *J. Geophys. Res.* **91**, (A2), 1417 (1986).
7. Y. D. Jia *et al.*, *Astrophys. J.* **696**, L56 (2009).

8. H. Lammer *et al.*, *Planet. Space Sci.* **54**, 1445 (2006).
9. S. Barabash *et al.*, *Nature* **450**, 650 (2007).
10. The bipolar signature in our rotated coordinate system is in the B_y component here instead of the B_z component, as it would be in the usual coordinate system used for a terrestrial magnetotail plasmoid (*18*).
11. T. L. Zhang *et al.*, *Geophys. Res. Lett.* **37**, L14202 (2010).
12. An earlier study found a flux rope in the Venus tail, but reconnection was rejected as a possible source because of the inconsistent orientation of the rope axis (*19*). In our case, the axis is consistent with reconnection. Flux ropes that have been seen on the nightside of Venus are much larger than those in the dayside ionosphere (*20*) and cannot explain these

micro-ropes, which appear not to have a magnetic reconnection source (*21*).
13. T. L. Zhang *et al.*, *Nature* **450**, 654 (2007).
14. C. T. Russell, O. Vaisberg, in *Venus*, D. M. Hunten, L. Colin, T. M. Donahue, V. I. Moroz, Eds. (Univ. of Arizona Press, Tucson, AZ, 1983), pp. 873–940.
15. J. L. Phillips, D. L. McComas, *Space Sci. Rev.* **55**, 1 (1991).
16. A. Fedorov *et al.*, *J. Geophys. Res.* **116**, (A7), A07220 (2011).
17. V. Angelopoulos *et al.*, *Science* **321**, 931 (2008).
18. M. B. Moldwin, W. J. Hughes, *J. Geophys. Res.* **96**, (A8), 14051 (1991).
19. J. A. Slavin *et al.*, *Geophys. Res. Lett.* **36**, L09106 (2009).
20. C. T. Russell, R. C. Elphic, *Nature* **279**, 616 (1979).

21. H. Y. Wei, C. T. Russell, T. L. Zhang, M. K. Dougherty, *Icarus* **206**, 174 (2010).
22. T. L. Zhang *et al.*, *Planet. Space Sci.* **54**, 1336 (2006).
23. S. Barabash *et al.*, *Planet. Space Sci.* **55**, 1772 (2007).

Ancient Impact and Aqueous Processes at Endeavour Crater, Mars

S. W. Squyres,[1]* R. E. Arvidson,[2] J. F. Bell III,[3] F. Calef III,[4] B. C. Clark,[5] B. A. Cohen,[6] L. A. Crumpler,[7] P. A. de Souza Jr.,[8] W. H. Farrand,[5] R. Gellert,[9] J. Grant,[10] K. E. Herkenhoff,[11] J. A. Hurowitz,[4] J. R. Johnson,[12] B. L. Jolliff,[2] A. H. Knoll,[13] R. Li,[14] S. M. McLennan,[15] D. W. Ming,[16] D. W. Mittlefehldt,[16] T. J. Parker,[4] G. Paulsen,[17] M. S. Rice,[1] S. W. Ruff,[3] C. Schröder,[18] A. S. Yen,[4] K. Zacny[17]

The rover Opportunity has investigated the rim of Endeavour Crater, a large ancient impact crater on Mars. Basaltic breccias produced by the impact form the rim deposits, with stratigraphy similar to that observed at similar-sized craters on Earth. Highly localized zinc enrichments in some breccia materials suggest hydrothermal alteration of rim deposits. Gypsum-rich veins cut sedimentary rocks adjacent to the crater rim. The gypsum was precipitated from low-temperature aqueous fluids flowing upward from the ancient materials of the rim, leading temporarily to potentially habitable conditions and providing some of the waters involved in formation of the ubiquitous sulfate-rich sandstones of the Meridiani region.

After more than 7 years in operation and 33 km of traversing, the Mars Exploration Rover Opportunity has reached Endeavour Crater. Endeavour is ~22 km in diameter and formed in Noachian (*1*) materials that predate

[1]Department of Astronomy, Cornell University, Ithaca, NY 14853, USA. [2]Department of Earth and Planetary Sciences, Washington University, St. Louis, MO 63031, USA. [3]School of Earth and Space Exploration, Arizona State University, Tempe, AZ 85287, USA. [4]Jet Propulsion Laboratory, California Institute of Technology, Pasadena, CA 91109, USA. [5]Space Science Institute, Boulder, CO 80301, USA. [6]NASA Marshall Space Flight Center, Huntsville, AL 35812, USA. [7]New Mexico Museum of Natural History & Science, Albuquerque, NM 87104, USA. [8]Human Interface Technology Laboratory, University of Tasmania, Launceston TAS 7250, Australia. [9]Department of Physics, University of Guelph, Guelph, Ontario N1G 2W1, Canada. [10]Center for Earth and Planetary Studies, Smithsonian Institution, Washington, DC 20560, USA. [11]U.S. Geological Survey, Astrogeology Science Center, Flagstaff, AZ 86001, USA. [12]Applied Physics Laboratory, Johns Hopkins University, Laurel, MD 20723, USA. [13]Botanical Museum, Harvard University, Cambridge, MA 02138, USA. [14]Department of Civil, Environmental, and Geodetic Engineering, Ohio State University, Columbus, OH 43210, USA. [15]Department of Geosciences, State University of New York, Stony Brook, NY 11794, USA. [16]Astromaterials Research and Exploration Science (ARES), NASA Johnson Space Center, Houston, TX 77058, USA. [17]Honeybee Robotics & Spacecraft Mechanisms Corporation, Pasadena, CA 91103, USA. [18]Universität Bayreuth und Eberhard Karls Universität, 72076 Tübingen, Germany.

*To whom correspondence should be addressed. E-mail: squyres@astro.cornell.edu

the sulfate-rich sedimentary rocks explored by Opportunity for most of its mission (*2*, *3*). Endeavour was chosen as a target because the rocks there record an ancient epoch in martian history, and because orbital infrared data show that phyllosilicate minerals are present in portions of the crater rim (*4*).

Opportunity arrived at Endeavour Crater on sol 2681 (*5*) of its mission, at a low-lying segment of the rim, ~700 m in length, named Cape York (Fig. 1). Shoemaker Ridge (*6*) forms the spine of Cape York and is the type locality for the Noachian materials of the rim, which we call the Shoemaker formation. Opportunity first arrived at Spirit Point, the southern tip of Cape York, and then traversed northward 851 m before stopping at Greeley Haven (*7*) at the northern end of Cape York to spend the martian winter.

Instruments of Opportunity's Athena payload (*8*, *9*) were used to investigate materials within the Shoemaker formation, including the bedrock outcrop Chester Lake (Fig. 2) near the southern end of Shoemaker Ridge, and several bedrock targets near Greeley Haven at the northern end. Although separated by more than half a kilometer, these outcrops are similar in physical appearance and elemental chemistry; we interpret them to represent the dominant surface rock type of Cape York.

Chester Lake and all the rocks near Greeley Haven have similar textures. They are brecciated, with dark, relatively smooth angular clasts up to ~10 cm in size embedded in a brighter, fractured, fine-grained matrix. Some outcrops, notably Chester Lake, show fine-scale lineations in the matrix and alignment of some clasts (Fig. 2). Pancam spectra of the matrix exhibit a gradual decrease in reflectance toward 1000 nm. The clasts can show specular reflections, have a relatively deep absorption at 934 nm, and have a shallower 535-nm absorption than the matrix materials, consistent with relatively unoxidized basaltic material containing low-Ca pyroxene.

The matrix of Chester Lake is easily abraded. A portion of Chester Lake dominated by matrix was abraded to a depth of ~2.5 mm with the rover's Rock Abrasion Tool (RAT). Resistance to abrasion is quantified using specific grind energy, the energy required to abrade away a unit volume of rock. The specific grind energy for Chester Lake was ~1.5 J mm^{-3}. Representative values for weak terrestrial materials are 0.7 to 0.9 J mm^{-3} for chalk and 4.8 to 5.3 J mm^{-3} for gypsum (*10*). Chester Lake is substantially weaker than all but 1 of the 14 diverse rocks abraded by Spirit at Gusev Crater (*11*) but is comparable to the sulfate-rich sandstones at Opportunity's landing site (*12*).

At Chester Lake, we used the Alpha Particle X-Ray Spectrometer (APXS) to measure the elemental composition of both the matrix (after abrasion by the RAT) and one of the clasts. Measurements were also made of three targets near Greeley Haven: Transvaal and Boesmanskop (both matrix) and Komati (a clast). All are similar to one another in composition, and all are similar to the basaltic sand typical of the Meridiani region (Table 1). The major elements (Na, Mg, Al, Si, Ca, and Fe) are mostly within 10 weight percent (wt %) of the basaltic sand composition, and all but a few are within 20 wt %.

Fe/Mn ratios of the matrix range from 40 to 44, and "Mg numbers" [$100 \times$ molar Mg/(Mg + Fe)] of all samples range from 41 to 48. These are within the ranges of basaltic meteorites from Mars [Fe/Mn ratios, 36 to 45; Mg numbers, 24 to 68 (fig. S1)] and indicate that any alteration of the protolith of these rocks did not substantially mobilize Mg, Mn, or Fe. P contents are higher than